Synergistic effect of reduced graphene oxide/azo-polymer layers on electrochemical performance and application as nonenzymatic chemiresistor sensors for detecting superoxide anion…

Article · October 2019

DOI: 10.1016/j.jelechem.2019.113520

CITATIONS
0

READS
30

4 authors:

André Olean-Oliveira
São Paulo State University
8 PUBLICATIONS **7** CITATIONS
SEE PROFILE

Jessica Pacheco
São Paulo State University
2 PUBLICATIONS **0** CITATIONS
SEE PROFILE

Patricia Seraphim
São Paulo State University
41 PUBLICATIONS **522** CITATIONS
SEE PROFILE

Marcos F. S. Teixeira
São Paulo State University
108 PUBLICATIONS **1,403** CITATIONS
SEE PROFILE

Journal of Electroanalytical Chemistry 852 (2019) 113520

Contents lists available at ScienceDirect

Journal of Electroanalytical Chemistry

journal homepage: www.elsevier.com/locate/jelechem

Synergistic effect of reduced graphene oxide/azo-polymer layers on electrochemical performance and application as nonenzymatic chemiresistor sensors for detecting superoxide anion radicals

André Olean-Oliveira [a], Jéssica C. Pacheco [a], Patricia M. Seraphim [b], Marcos F.S. Teixeira [a,*]

[a] Department of Chemistry and Biochemistry School of Science and Technology - Sao Paulo State University (UNESP) Rua Roberto Simonsen 305, CEP 19060-900, Presidente Prudente, SP, Brazil

[b] Department of Physiotherapy School of Science and Technology - Sao Paulo State University (UNESP) Presidente Prudente, SP, Brazil

ARTICLE INFO

Keywords:
Azo-polymer
Graphene
Pi-conjugation
Chemiresistor
Superoxide detection
Chrono-impedance

ABSTRACT

The present paper describes a nonenzymatic chemiresistor sensor based on an azo-polymer and reduced graphene oxide (rGO) as a resistive platform for superoxide radical detection. The sensorial platform was prepared on layer-by-layer-assembled films of poly(azo-Bismarck Brown Y) and reduced graphene oxide by cyclic voltammetry. The nanocomposite film exhibited interesting synergetic properties based on the redox properties of the azo-polymer combined with the good electronic conductivity and stability of graphene. The electrical conductivity mechanism of the graphene-polymer was analyzed by electrochemical impedance and compared to that of an electrode coated with only polymer. The conductance properties of the interlayer formed by π-π stacking between the conjugated structure of the polymer chains and the structure of the graphene sheet are dependent on the applied potential of the system. The performance of the poly(azo-BBY)/rGO film as a chemiresistor material for the sensing of superoxide anions was evaluated by impedance measurements at the applied potential of +0.30 in PBS (7.4). The charge transfer resistance values change substantially in the presence of superoxide in solution. The effect of superoxide on the resistivity of the device is attributed to changes in the oxidation state of the polymer. The impedance measurements in real time (chrono-impedance) with the poly(azo-BBY)/rGO sensor with different superoxide concentrations revealed good linearity behavior between the real impedance and the superoxide anion concentration (0.12–2.6 mmol L^{-1}) with a detection limit of 81.0 μmol L^{-1}.

1. Introduction

Currently, the use of carbonaceous materials, such as graphene oxides, carbon nanofibers and carbon nanotubes, has been reported for construction of chemiresistor sensors [1–6]. The incorporation of graphene into these devices is attractive due its to excellent electronic transport properties, broadly adaptable surface area, excellent thermal conductivity and high mechanical resistance [7,8]. In addition, the attachment of graphene to other materials, such as conductive polymers, can improve the physico-chemical properties of the device through the functional synergy of the two combined materials [9,10]. The properties of these nanocomposites depend on the graphene, the polymer type and the methodology of preparation [11]. Studies have shown that graphene together with conductive polymers generates an interconnected conducting network and three-dimensional porous microstructures. These represent ideal conditions for the elaboration of sensorial platforms for the development of chemical sensors [12,13].

Reactive oxygen species (ROS) are the intermediary products of oxygen metabolism reactions occurring in mitochondria under physiological conditions of aerobic cellular metabolism [14]. These intermediate species formed during metabolism are highly reactive: when present in excess in the living organism, oxidative stress can cause the destruction of proper functioning of living tissues, inflammation and cancer. Therefore, the detection and quantification of ROS are extremely important [15,16]. In comparison with other methods for superoxide radical detection [17–20], the electrochemical method can be considered one of the promising strategies due to its simplicity, low-cost instrumentation, fast response, low detection limit and ease of use [21]. Thus, electrochemical sensors have been extensively developed for the determination of ROS [22–26]. However, many studies have described electrochemical ROS

* Corresponding author.
E-mail address: marcos.fs.teixeira@unesp.br (M.F.S. Teixeira).

https://doi.org/10.1016/j.jelechem.2019.113520
Received 8 August 2019; Received in revised form 23 September 2019; Accepted 24 September 2019
Available online 6 October 2019

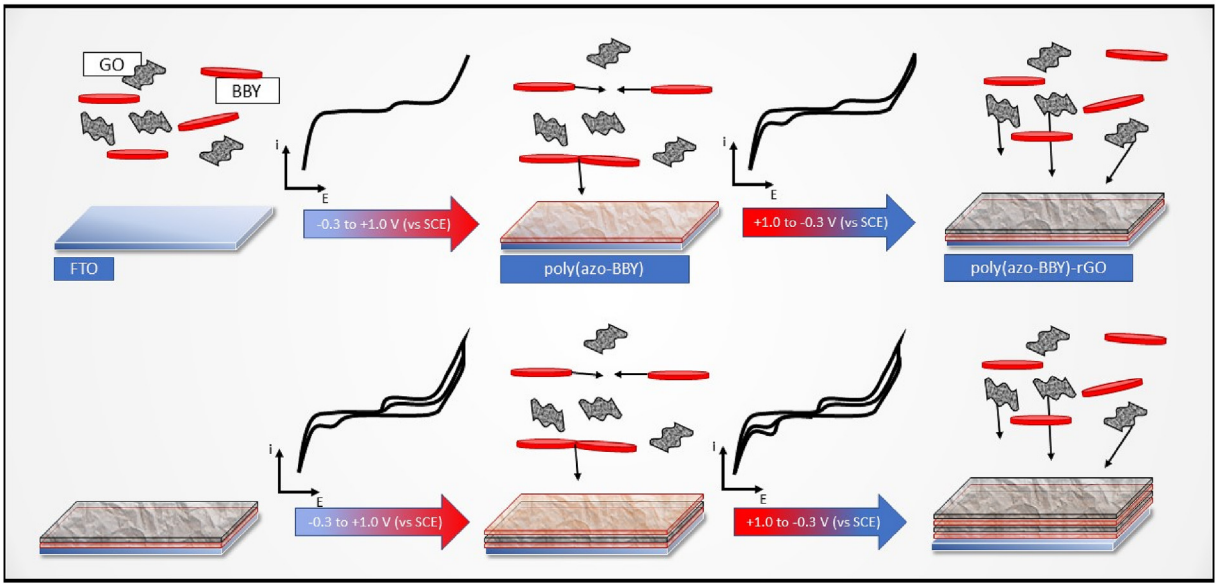

Scheme 1. Schematic illustration of the sensor construction of poly(azo-BBY)-rGO film. BBY = Bismarck Brown Y; GO = graphene oxide.

sensors using the dismutase superoxide enzyme [27,28]. Among the electrochemical sensors are chemiresistors that are considered as attractive platforms for chemical sensing. The analytical signal is based on the change in the electrochemical impedance of the material due to chemical interaction with the analyte.

Here, we present the development of a chemiresistor sensor with integrated-sensing function based on a hybrid nanocomposite of poly(azo-Bismarck Brown Y) and rGO. The resultant composite was characterized by electrochemical properties, nanostructure and impedance spectroscopy. Equivalent circuit models were adopted as an approach to elucidate the physico-chemical properties and the overall impedance in the device. The sensor response to different superoxide anion concentrations reveals that the resistance of the polymer is sensitive in the presence of $O_2^{\bullet-}$ in solution. In future, the sensor will be employed to measure in real time the rates of mitochondrial superoxide release in skeletal muscles upon stimulation with sequential substrate addition protocols [29].

2. Materials and methods

All electrochemical measurements were performed in a conventional electrochemical cell containing three electrodes: a saturated calomel electrode (SCE) as the reference; platinum wire as the counter electrode and a fluoride-doped tin oxide (FTO) electrode as the working electrode (1.0 cm^2). The impedance measurements were performed with Palsens3 interfaced PSTrace 5.2 software. The reagents used were of high purity ≥98% (Sigma Aldrich).

The FTO surface was washed in isopropanol before being coated with nanocomposite. The sensorial platform based on poly(azo-Bismarck Brown Y)-rGO was prepared as described by Olean-Oliveira and Teixeira [13]. To the FTO surface, was applied a potential cycling between −0.30 and + 1.00 V (vs. SCE) for 20 cycle scans at a scan rate of 10 mV s^{-1} in deaerated aqueous solution (0.1 mol L^{-1} HCl) containing 10 mmol L^{-1} of Bismarck Brown Y (4,4′-(*m*-phenylenebisazo)bis-*m*-phenylenediamine - BBY) and 1.00 mg mL^{-1} of graphene oxide

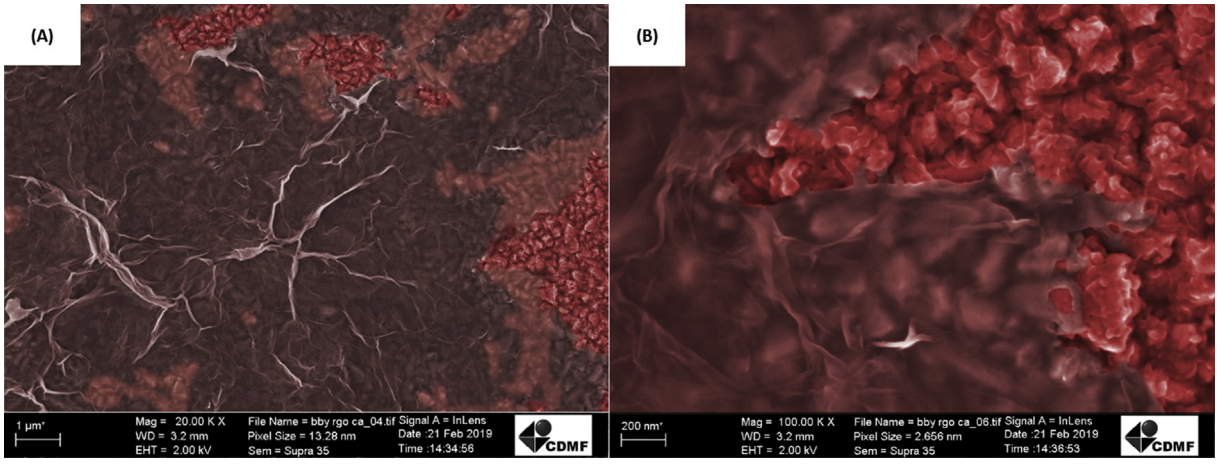

Fig. 1. SEM images of artificially colored nanocomposite film of poly(azo-BBY)-rGO at magnification of (**A**) 50,000× and (**B**) 100,000×. The reduced graphene oxide and polymer were colored with gray and red shades, respectively.

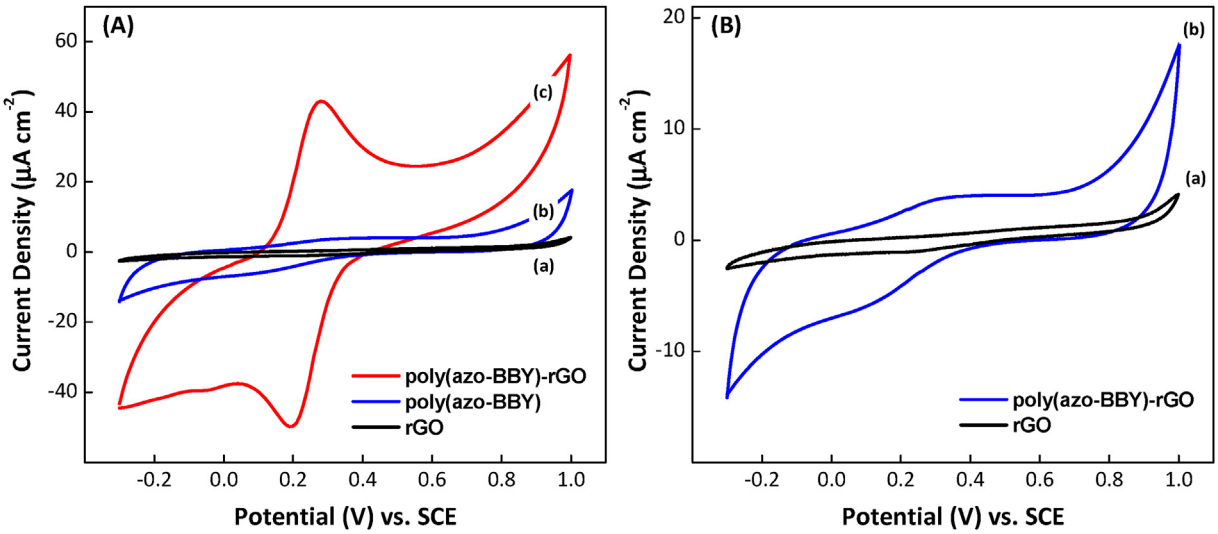

Fig. 2. (**A**) Voltammetric response to FTO coated with rGO (curve **a**), poly(azo-BBY) (curve **b**) and poly(azo-BBY)-rGO (curve **c**) in KCl 0.50 mol L^{-1} (pH 2.0) solution under N_2 atm. (**B**) The magnified view of the voltammetric response to FTO-coated rGO (curve **a**) and poly(azo-BBY) (curve **b**). Scan rate = 25 mV s^{-1}.

(Sigma-Aldrich). After coating, the platform was washed abundantly with deionized water and a potential of −0.30 V (vs. SCE) was applied for 1 h in 0.50 mol L^{-1} KCl solution (pH 2.00). The mechanism of film formation is illustrated in Scheme 1. The coated FTO electrode was prepared on layer-by-layer assembled films which were composed of poly(azo-BBY) for anodic scan and reduced graphene oxide for cathodic scan. An electrode coated only with poly(azo-BBY) was prepared under the same conditions for comparative analysis. The active area of the FTO/poly(azo-BBY) and FTO/poly(azo-BBY)-rGO electrodes was calculated based on the ratio $\Gamma = Q/nFA$. Where Q is the charge obtained by integrating the area of anode current values as a function of the scan time with baseline correction (C), the number of electrons involved (n = 2e^-), F the Faraday constant (96485 C mol/e^-) and A the electrode area (1.0 cm^2). The coated electrodes were submitted the electrochemical redox cycling in KCl solution (0.50 mol L^{-1}; pH 2.0) solution under nitrogen gas at a scan rate of 5 mV s^{-1}.

The charge transfer resistance of the coated electrodes was investigated using EIS measurements at an applied potential of −0.30 V (vs. SCE) in a solution of 0.5 mol L^{-1} KCl (pH 2.0). The pH of the electrolytic solution was adjusted with concentrated hydrochloridric acid. The EIS measurements were performed through the incidence of a sine wave of 10 mV applied over a frequency range of 50 kHz to 0.1 Hz with 10 steps/dec. All spectra were recorded at 25 °C. The analysis of the complex plane impedance spectra was determined by ZPlot 2.4 software. The analytical curve was obtained by chrono-impedance measurements using the chemiresistor sensor in 0.05 mol L^{-1} phosphate buffer solution (pH 7.4) at a fixed frequency of 0.1 Hz and at an applied potential of −0.30 V vs. SCE. All aqueous solutions were deaerated with N_2 gas.

3. Results and discussion

Fig. 1 shows the image of the poly(azo-BBY)-rGO film surface obtained by scanning electron microscopy (SEM) and artificially colored. It was possible to clearly verify the reduced graphene oxide sheet on the polymer film of poly(azo-BBY) (see Fig. 1A). In Fig. 1B, with an increased magnitude of magnification, a rough and uniform polymer structure distributed over the electrode can be seen, similar to that reported by Teixeira and collaborators [30] for a poly(azo-Bismark Y) film constructed under similar conditions.

Fig. 2 shows the cyclic voltammetric behavior of the FTO coated with rGO (a), poly(azo-BBY) (b) and poly(azo-BBY)-rGO (c) in 0.50 mol L^{-1} KCl solution (pH 2.0) at a scan rate of 25 mV s^{-1}. The electrochemical response for both films containing poly(azo-BBY) showed a characteristic redox pair of the azo-polymer, assigned for the oxidation and reduction of the azo group moiety in the molecule [12,13,30].

No significant redox process of the electrode coated only with graphene was observed in the potential range studied. However, there are reports in the literature describing a low-resolution redox pair due to the oxygen and phenolic groups remaining on the structure of electrodeposited graphene oxide [31,32]. This behavior indicates that the electrochemical reduction of graphene oxide was successful during its electrodeposition at the FTO surface. The significant increase in the current values for the poly(azo-BBY)-rGO (I_{AP} = +36.0 and I_{CP} = −43.0 μA cm^{-2}) was verified in comparison to the poly(azo-BBY) (I_{AP} = +0.98 and I_{CP} = −6.32 μA cm^{-2}). Similar behavior of current increase was observed for mixed polyaniline with rGO [6]. The introduction of graphene into the polymer matrix increased the magnitude of peak current, which may be related to the activation of azo active sites present from the outer to the inner layers of the film. The active area of the electrode coated with poly(azo-BBY)-rGO (1.29 nmol cm^{-2}) was 21.5 times greater than that of the electrode containing only the redox polymer (0.06 nmol cm^{-2}). In addition, its redox process presented better definition, with a decrease in the ΔE_P value ($E_{AP} - E_{CP}$ = 0.08 V) indicating a reversible redox system. Similar results of the electrochemical performance of conducting polymers with the insertion of graphene derivatives in the structure are reported in the literature as supercapacitors [6,33]. The existence of the synergistic effect between graphene and poly(azo-BBY) is related to the filling of the space and gaps between the portions of graphene sheets with conducting polymer. This interaction involves the interlayer formed by π-π stacking between the conjugated structure of the polymer chains and the structure of the graphene sheet [12,34].

The electrochemical impedance spectroscopy results of electrodes coated with poly(azo-BBY) and poly(azo-BBY)-rGO were investigated to analyze important information about the interfacial properties of the obtained films. The spectra were obtained at two applied potentials (−0.30 V and +0.30 V *vs.* SCE) in 0.5 mol L^{-1} KCl (pH 2.0) under N_2 atmosphere, as represented in Fig. 3A and B, respectively. These applied potentials were chosen because they are coincident with the reduction and oxidation of azo groups of the polymer, as previously observed in the voltammograms. The equivalent circuit models (ECMs) used for the

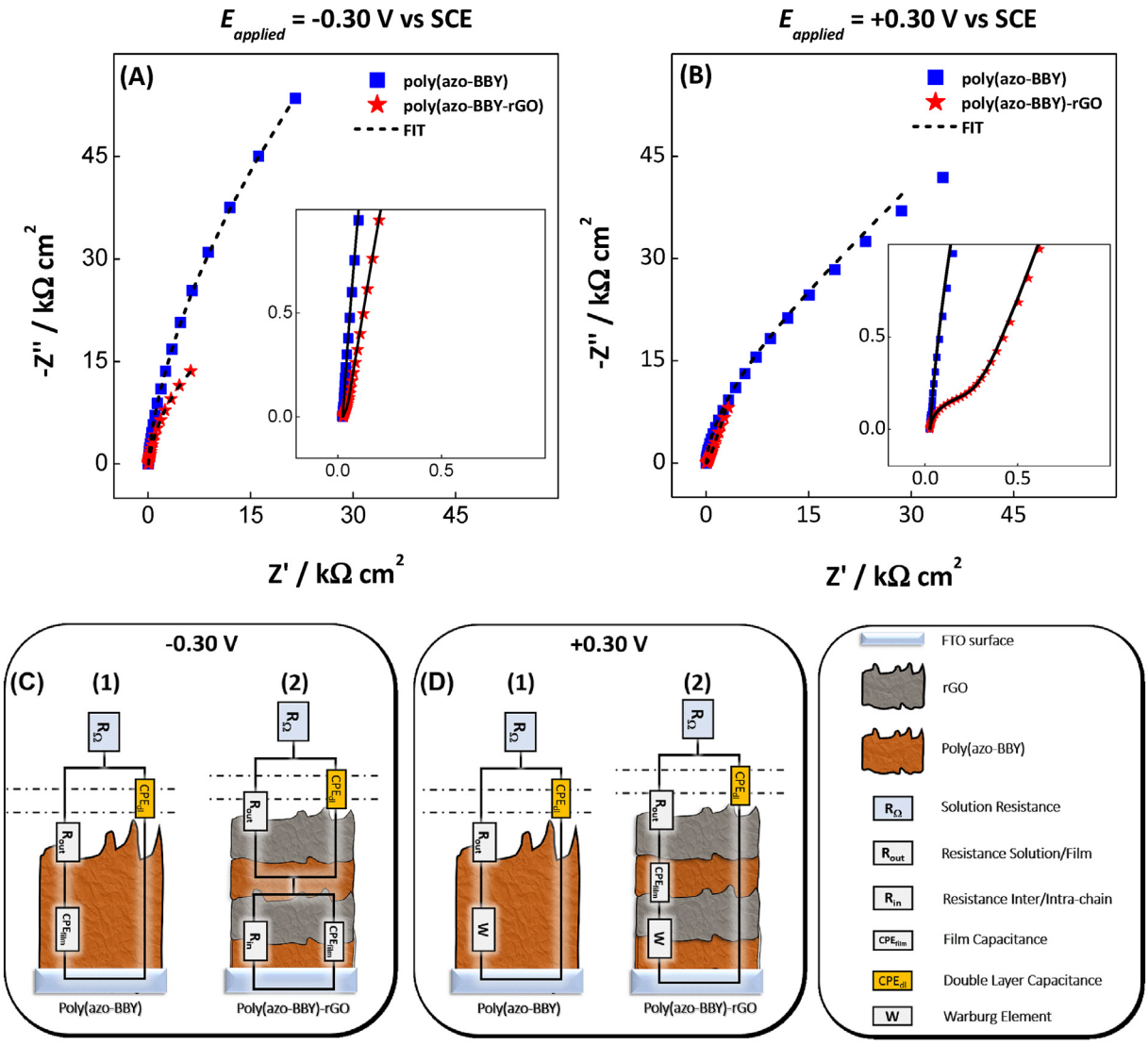

Fig. 3. Electrochemical impedance profiles for the electrodes coated with poly(azo-BBY) (blue square) and poly(azo-BBY)-rGO (red star) in 0.5 mol L^{-1} KCl (pH 2.0) in the absence of O_2. **Fig.** (**A**) = applied potential at −0.30 V (vs. SCE). **Fig.** (**B**) = applied potential at +0.30 V (vs. SCE). The ECMs used for fitting the impedance spectra are represented in figures (**C**) and (**D**) for each applied potential, respectively.

Table 1
Physico-chemical parameters determined from fitting of the electrochemical impedance spectra of the poly(azo-BBY) and poly(azo-BBY)-rGO films using ECMs shown in Fig. 3C and D. $R_\Omega = 27\ \Omega\ cm^2$. The fitting error is ≤ 2%. pH = 2.0

Film	R_{out}	R_{in}	CPE_{dl}	α_{dl}	CPE_{film}	α_{film}	W	ECMs
	(kΩ cm^2)		μF cm^{-2} $s^{\alpha-1}$		μF cm^{-2} $s^{\alpha-1}$		kΩ $s^{-0.5}$ cm^2	
				−0.30 V (vs. SCE)				
p(azo-BBY)	63.5	–	21.1	0.96	12.1	0.69	-	Fig. 3C1
p(azo-BBY)-rGO	0.02	53.0	93.7	0.90	310	0.75	-	Fig. 3C2
				+0.30 V (vs. SCE)				
p(azo-BBY)	22.1	–	13.7	0.95	–	–	32.6	Fig. 3D1
p(azo-BBY)-rGO	0.27	–	12.5	0.97	185	0.81	0.55	Fig. 3D2

mathematical adjustments of the obtained spectra are illustrated in Fig. 3C and D. Together with Table 1, the impedance parameters are obtained from the proposed equivalent electrical circuits. According to Lvovich [35], the ECMs for redox polymer-coated electrodes are composed of numerous electrical components. The assignment of ideal electrical elements is dependent on the polymer morphology, the polymer redox properties, the double layer, the diffusion of the electrolytic solution within the polymer matrix, and the redox-active moieties. In this work, the ECMs for both coated electrodes demonstrated similar electrical solution resistance (R_Ω) in series with a parallel circuit consisting of charge transfer resistance of the film/solution interface (R_{out}) and a constant phase element relating to the capacitance of the electric

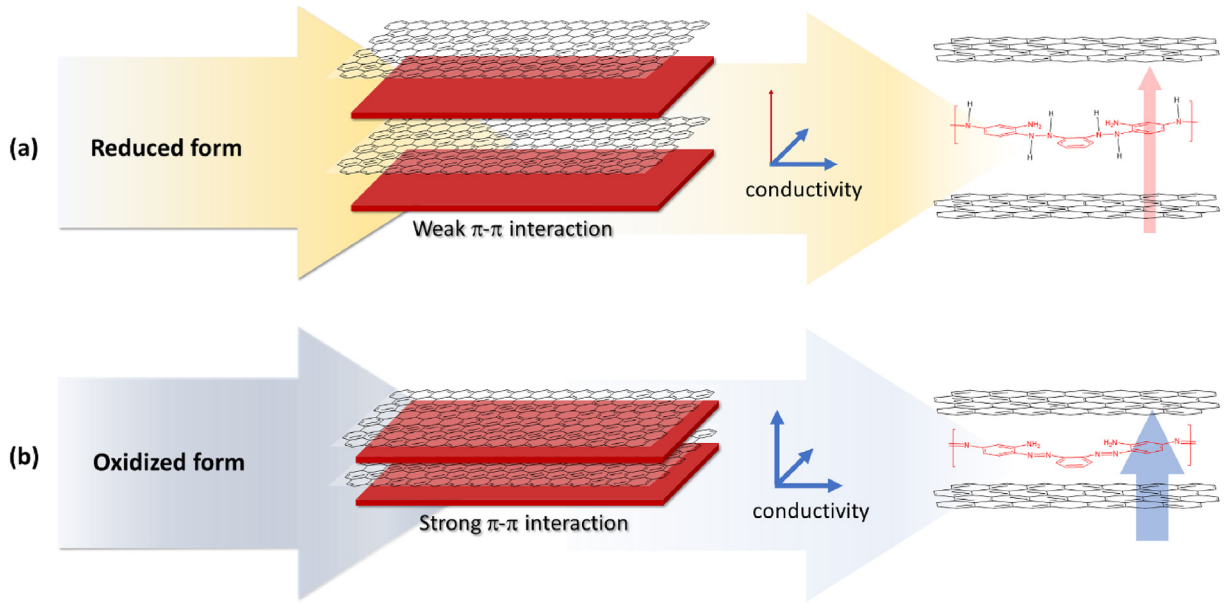

Scheme 2. Active control of molecular orientation and molecular anisotropy according to the applied potential: **(a)** −0.30 V and **(b)** +0.30 V vs. SCE.

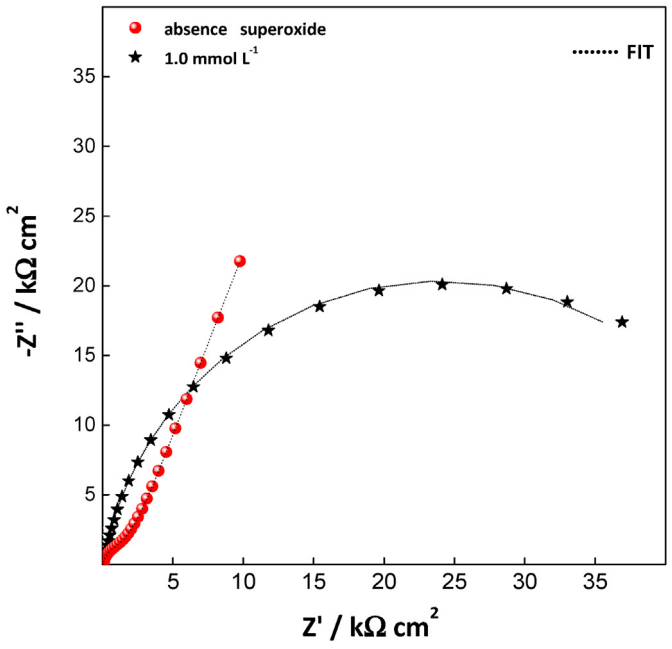

Fig. 4. Electrochemical impedance profile of the chemiresistor sensor in the absence (red circle) and presence (black star) of superoxide (1.0 mmol L^{-1}) in PBS (pH 7.4). $E_{applied}$ = +0.30 V (vs. SCE). The ECMs used for fitting the complex plane impedance are represented in Fig. 3D2.

double layer (CPE_{dl}). The constant phase element (CPE) is a non-ideal capacitor and its impedance is given by (Eq. (2)):

$$CPE = \frac{1}{Q(j\omega)^{\alpha}} \quad (2)$$

where the α exponent has values between 0 and 1. For n = 1, CPE has a perfect capacitor behavior, and Q has units of capacitance. When n ≠ 1, the Q has units of $F/s^{(1-\alpha)}$. The *j* represents complex-plan and ω the angular frequency (s^{-1}).

Table 2
Parameters obtained from fitting of electrochemical impedance spectra of the chemiresistor sensor in Fig. 4. The errors presented for the fit were all below 2%.

Superoxide content of solution mmol L^{-1}	R_{out} kΩ cm^2	CPE_{dl} μF cm^{-2} $s^{\alpha-1}$	α_{dl}	CPE_{film} μF cm^{-2} $s^{\alpha-1}$	α_{film}	W kΩ $s^{-0.5}$ cm^2
0.0	2.73	12.8	0.94	185	0.75	0.55
1.0	41.0	16.9	0.89	457	0.76	0.12

For the electrode coated only with poly(azo-BBY) at the applied potential of −0.30 V, a second constant phase element (CPE_{film} = 12.1 μF cm^{-2} $s^{\alpha-1}$) was observed in series with R_{out}. This constant phase element is related to the proton insertion in the polymer matrix, generating a load capacitor. Conductive polymers generally exhibit the impedance behavior of a capacitor [36–38]. The poly(azo-BBY)-rGO film displayed a high value of CPE_{film} (310 μF cm^{-2} $s^{\alpha-1}$) in parallel with a second charge transfer resistance (R_{in}) associated with the rGO/poly(azo-BBY) interface. The high CPE_{film} is attributed to the capacitive properties of graphene in the formed film layers [39,40]. The R_{out} decreased substantially in relation to the electrode coated only with poly(azo-BBY), indicating the effect of electronic communication of the graphene-polymer/solution interface. As an overview, other impedance parameters obtained for the poly(azo-BBY)-rGO nanocomposite at applied potential of −0.30 V are related to the oxidation state of the polymer. At this potential, the polymer (reduced state) is a semi-conjugated system and the band gap is maximized, as shown by Scheme 2**a**. It is noteworthy that the oxidation state changes of the azo-moieties on the polymer could result in a less feasible pi-pi interaction between RGO nanosheets and polymer film. The increase in the tunneling barrier of azo-polymer decreases conductance for electron transfer, resulting in increased resistance of the basal graphene plane/polymer interface (R_{in} = 53 kΩ cm^2).

At +0.30 V vs. SCE, the electrode coated with poly(azo-BBY) film showed the same ECM profile previously observed for the reduction potential, with only a substitution of constant phase element of the polymer (CPE_{film}) by Warburg impedance element (W) (see Fig. 3D1):

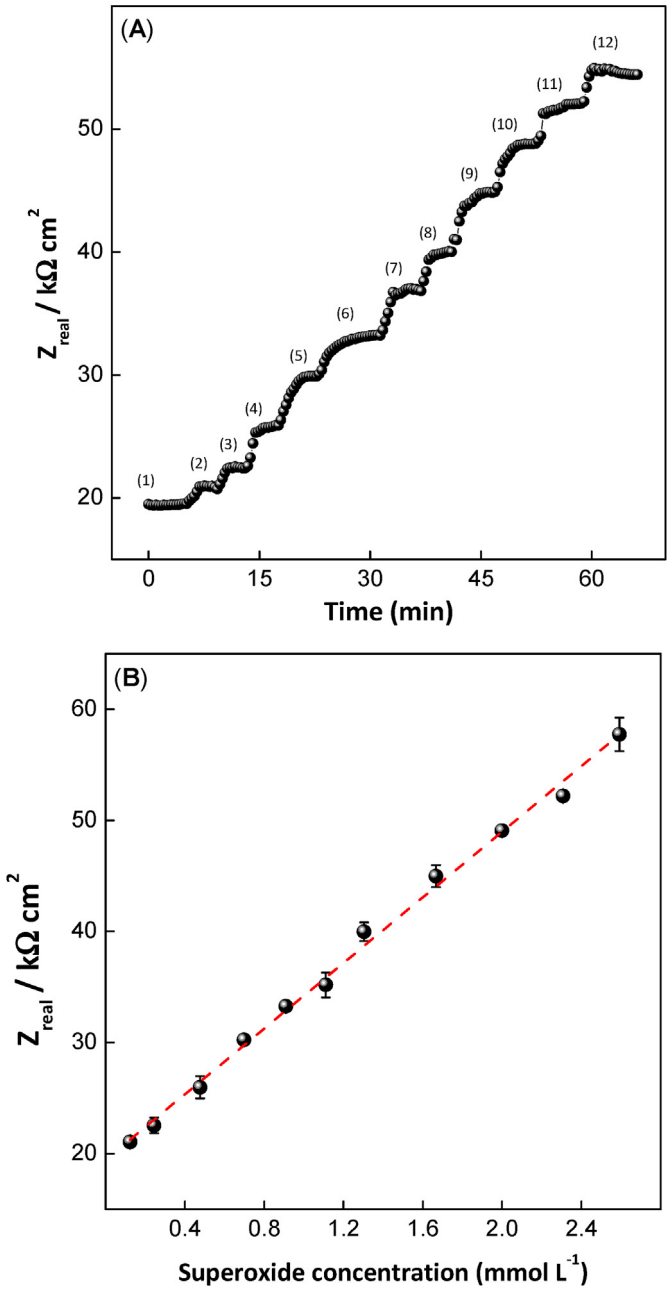

Fig. 5. (**A**) Chrono-impedance response of the chemiresistor sensor at different dissolved superoxide concentrations in 0.05 mol L^{-1} PBS (pH 7.4). Applied frequency = 0.10 Hz. Applied potential = +0.30 V (*vs.* SCE). Superoxide ion concentrations = 0.00 (1); 0.12 (2); 0.24 (3); 0.48 (4); 0.70 (5); 0.91 (6); 1.1 (7); 1.3 (8); 1.7 (9); 2.0 (10); 2.3 (11); and 2.6 mmol L^{-1} (12). (**B**) Calibration curve for the chemiresistor sensor as a function of superoxide concentration. The error bars represent the standard deviation from three separate experiments using the same sensor.

$$W = \frac{1}{\sigma\sqrt{j\omega}} \quad (3)$$

where σ is the Warburg coefficients and ω is the angular frequency (s^{-1}). The Warburg impedance element is due to the presence of diffusional control of the ions through the polymer matrix and the charge accumulation at low frequencies [38,41]. For this potential, the extended π-conjugation of the poly(azo-BBY) film is maximal (Scheme 2**b**), resulting in a decrease in resistance of the polymer interface (R_{out} = 22.1 kΩ cm^2).

Table 3
Comparison of the detection limit to different superoxide sensors.

Sensorial platform	Detection method	Detection limit (mol L^{-1})	Ref.
Cu-complex/Pt	Amperometric	1.5×10^{-7}	[42]
Pt–Pd/MWCNTs-SOD	Amperometric	7.1×10^{-7}	[23]
SOD/CNT/GCE	Amperometric	8.1×10^{-5}	[43]
SOD/CNT/PEDOT/GCE	Amperometric	1.0×10^{-6}	[43]
PDDA/MWCNTs–Pt/GCE	Amperometric	1.0×10^{-7}	[25]
poly(azo-BBY)/rGO	Impedimetric	8.1×10^{-5}	Present Work

MWCNTs = Multi-walled carbon nanotubes; CNT = carbon nanotubes; PEDOT = poly(3,4-ethylenedioxythiophene); PDDA = Poly-diallyldimethylammonium; SOD = superoxide dismutase.

Comparatively, the impedance data obtained for the poly(azo-BBY)-rGO film at +0.30 V vs. SCE are shown as a complex plane plot in Fig. 3B. To analyze the characteristics of the impedance plot, an equivalent circuit (Fig. 3D2) composed of a solution resistance (R_Ω) in series with a parallel $CPE_{dl}/R_{out}CPE_{film}W$ combination was used to fit the spectra. The presence of a semicircle at high frequencies (kinetic control region) is due to slight oxidation of graphene on the film surface, and consequently an increase in resistance of the film/solution interface (0.27 kΩ cm^2) when compared with the same electrode at the reduction potential (0.02 kΩ cm^2). The CPE_{film} impedance response decreased significantly, with a small diffusion component W. The decrease of CPE value in the hybrid film results from the compaction of interlayers resulting from the effective π-π interactions between the graphene plane and azo-polymer (Scheme 2**b**). This synergistic effect results in an ad hoc network communication at the nanoscale.

4. Superoxide anion chemiresistor response

The performance of poly(azo-BBY)-rGO film as chemiresistor material for the sensing of superoxide anion was evaluated by impedance measurements at an applied potential of +0.30 V (vs. SCE) in 0.05 mol L^{-1} phosphate buffer solution (pH 7.4). The PBS was used as a support electrolyte to test device performance under biological conditions. Fig. 4 shows the complex plane impedance spectra of the chemiresistor sensor in the absence and presence of superoxide radical anion. To analyze the characteristics of the impedance plot, the equivalent circuit represented in Fig. 3D2 was used to fit the spectra. The resistance is related with the reaction between the conjugated polymer charge-transfer complex and

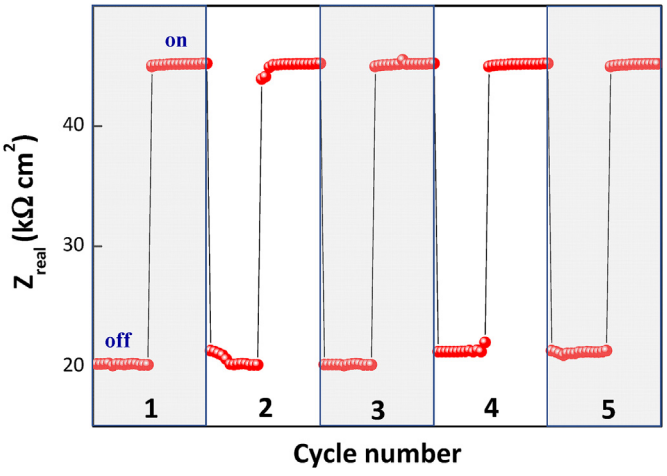

Fig. 6. Reversibility test of the chemiresistor sensor on/off response to a 2.0 mmol L^{-1} solution of superoxide in 0.05 mol L^{-1} PBS. Applied frequency = 0.10 Hz. Applied potential = +0.30 V (*vs.* SCE).

superoxide anion ($O_2^{\bullet-}$) in solution:

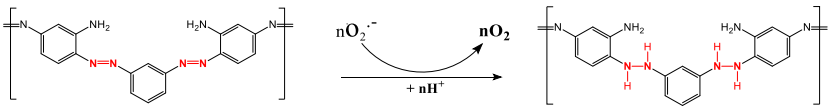

(4)

As shown in Table 2, the value of the resistance (R_{out}) changes substantially in the presence of superoxide in solution, indicating that the sensorial platform can be used to monitor levels of superoxide anion.

The effect of superoxide on the resistivity of the device is attributed to changes in oxidation state of polymer. The superoxide ion interacts with the polymer and reduces the pi-conjugation of poly(azo-BBY) film, resulting in increased electrical resistance at the graphene/polymer interface. The performance evaluation of the sensor response as a function of the superoxide ion concentration was realized by chrono-impedance at a fixed frequency of 1.0 Hz. The choice of the fixed frequency was analyzed according to the Bode diagram (plot not shown).

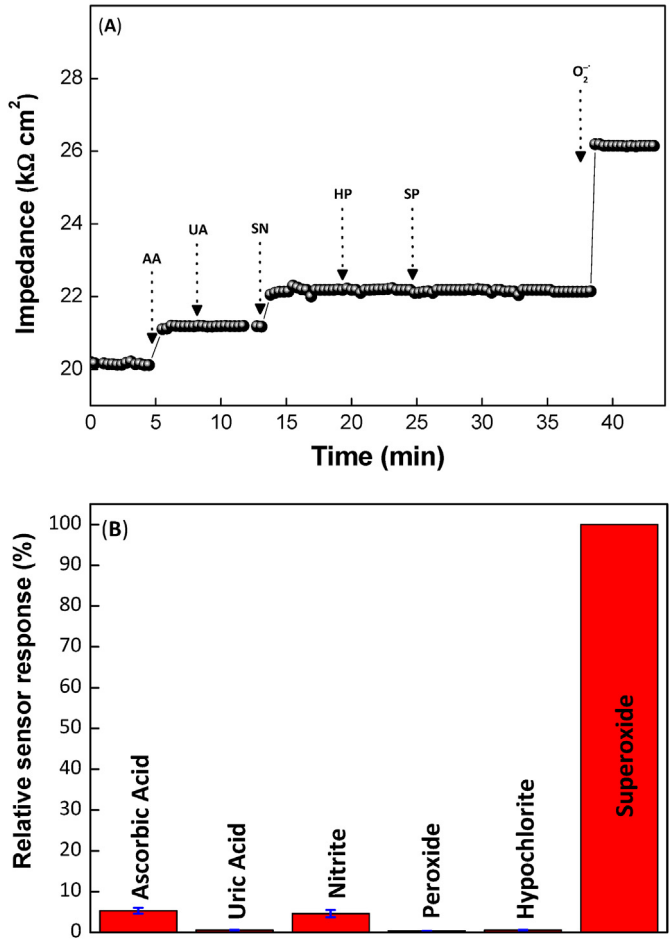

Fig. 7. (**A**) Chrono-impedance responses of sensor with successive additions of 0.10 mmol L^{-1} ascorbic acid (AA), uric acid (UA), sodium nitrite (SN), hydrogen peroxide (HP), sodium hypochlorite (SH) and superoxide ($O_2^{\bullet-}$) in 0.05 mol L^{-1} PBS. Applied frequency = 0.10 Hz. Applied potential = +0.30 V (*vs.* SCE). Additions of interference species in solution and their times are shown with arrows. (**B**) Relative selectivity percentage of sensor response (triplicate). The dates were based on Fig. (**A**).

The maximum changes in the impedance spectra are observed at frequencies below 5 Hz, which is the region most reflecting the resistance of the device. A typical response of the sensor, recorded at different superoxide ion concentrations in PBS, is represented in Fig. 5A. Changes in resistance of the device as a function of superoxide concentration in solution provide a straightforward sensor response of the studied phenomena.

Fig. 5B shows a linear relationship between the impedance magnitude and superoxide anion concentration in the range from 0.12 mmol L^{-1} to 2.6 mmol L^{-1}: *Real impedance* (kΩ cm^2) = 19.4 (±0.4) + 14.8 (±0.3) [$O_2^{\bullet-}$] (mmol L^{-1}) ($n = 11$; $r = 0.9956$) with a detection limit of 81.0 μmol L^{-1}. The detection limit was calculated by the equation $3s/b$, where s is the standard deviation of the device response in absence of the analyte and b is the slope of the analytical curve obtained by chrono-impedance. Table 3 lists the limit detection values reported in the literature for enzymatic and nonenzymatic sensors for superoxide anion. The detection limit of this electrochemical device is comparable to some scientific work using the amperometric detection method. However, this characteristic must be improved for a sensible development of this sensor in biological systems.

Fig. 6 shows the signal repeatability of the chemiresistor sensor determined during 5 cycles in PBS without and with superoxide anion. Upon switching to the 2.0 mmol L^{-1} superoxide solution, an increase in the impedance at 0.1 Hz is observed. Since the conduction behavior is based on the effect of polymer oxidation state, the increased presence of superoxide in solution in the reduced form polymer will increase the impedance of the film. Upon switching back to electrolytic solution without superoxide anion, the impedance returns to the original baseline value. The sensor exhibited good reproducibility and reversibility. The relative variation was of 1.6% in the overall response for repeated on/off cycles.

The response and recovery time were 1.3 ± 0.6 s and 1.0 ± 0.5 s, respectively. The selectivity of the chemiresistor sensor was investigated by chrono-impedance by addition of ascorbic acid (AA), uric acid (UA), sodium nitrite (SN), hydrogen peroxide (HP) and sodium hypochlorite (SH) in phosphate buffer. As shown in Fig. 7A, there is a weak response when adding uric acid, peroxide and hypochlorite into the same concentration of superoxide ion solution. Only ascorbic acid and nitrite result in an impedance response due to reducing properties.

The relative sensor response (S_R) was evaluated by the following Eq. (5):

$$S_R = \left(\frac{\Delta S_i}{\Delta S_o}\right) x \ 100\% \qquad (5)$$

where ΔS_i is the difference in the impedance measurement with interference and ΔS_o is the difference in the impedance for superoxide. Fig. 7B shows the relative selectivity percentage in the impedance response of the sensor. The analyzed species were not considered interferences because the relative responses in the measured impedance were less than 5%. These results indicate that the chemiresistor sensor is a promising platform for superoxide detection, due to the selectivity presented for potential interferences present in a biological environment.

5. Conclusion

An increase in electrochemical performance was observed by the addition of reduced graphene oxide in the polymer matrix of poly(azo-Bismarck Brown Y), as observed by the techniques of cyclic voltammetry and electrochemical impedance spectroscopy. Overall, the electron transfer between polymer and superoxide changes the oxidation status of the poly(azo-BBY), and consequently the resistance of the device. This activity essentially allowed superoxide detection in solution. The chemiresistor sensor for selective monitoring of superoxide was effective and offers possible applications in biological systems.

Acknowledgment

The authors acknowledge FAPESP (2016/09017-1 and 2013/07296-2) for financial support. A.O.O. thanks CAPES-Brazil for a doctor fellowship. SJT and NSA ∴

References

[1] S. Nufer, M.J. Large, A.A.K. King, S.P. Ogilvie, A. Brunton, A.B. Dalton, Edge-selective gas detection using Langmuir films of graphene platelets, Acs Appl Mater Inter 10 (2018) 21740–21745.
[2] Y.H. Kim, K. Lee, H. Jung, H.K. Kang, J. Jo, I.K. Park, H.H. Lee, Direct immune-detection of cortisol by chemiresistor graphene oxide sensor, Biosens. Bioelectron. 98 (2017) 473–477.
[3] S. Pandey, Highly sensitive and selective chemiresistor gas/vapor sensors based on polyaniline nanocomposite: a comprehensive review, J. Sci. 1 (2016) 431–453.
[4] L.Z. Chen, M.C. Weng, P.D. Zhou, F. Huang, C.H. Liu, S.S. Fan, W. Zhang, Graphene-based actuator with integrated-sensing function, Adv. Funct. Mater. 29 (2019).
[5] S. Badhulika, T. Terse-Thakoor, C. Villarreal, A. Mulchandani, Graphene hybrids: synthesis strategies and applications in sensors and sensitized solar cells, Front Chem 3 (2015).
[6] M. Kim, C. Lee, J. Jang, Fabrication of highly flexible, scalable, and HighPerformance supercapacitors using polyaniline/reduced graphene oxide film with enhanced electrical conductivity and crystallinity, Adv. Funct. Mater. 24 (2014) 2489–2499.
[7] J. Phiri, P. Gane, T.C. Maloney, General overview of graphene: production, properties and application in polymer composites, Mater Sci Eng B-Adv 215 (2017) 9–28.
[8] S. Ren, P. Rong, Q. Yu, Preparations, properties and applications of graphene in functional devices: a concise review, Ceram. Int. 44 (2018) 11940–11955.
[9] A. Noel, J. Faucheu, M. Rieu, J.P. Viricelle, E. Bourgeat-Lami, Tunable architecture for flexible and highly conductive graphene-polymer composites, Compos. Sci. Technol. 95 (2014) 82–88.
[10] M.J. Deka, S.K. Sahoo, D. Chowdhury, p-Type and n-type azobenzene nanocluster immobilized graphene oxide nanocomposite, J. Photochem. Photobiol., A 372 (2019) 131–139.
[11] A.J. Marsden, D.G. Papageorgiou, C. Valles, A. Liscio, V. Palermo, M.A. Bissett, R.J. Young, I.A. Kinloch, Electrical percolation in graphene-polymer composites, 2D Mater. (2018) 5.
[12] A. Olean-Oliveira, T. Olean-Oliveira, A.C.R. Moreno, P.M. Seraphim, M.F.S. Teixeira, A chemiresistor sensor based on azo-polymer and graphene for real-time monitoring of mitochondrial oxygen consumption, ACS Sens. 4 (2019) 118–125.
[13] A. Olean-Oliveira, M.F.S. Teixeira, Development of a nanocomposite chemiresistor sensor based on pi-conjugated azo polymer and graphene blend for detection of dissolved oxygen, Sens. Actuators B Chem. 271 (2018) 353–357.
[14] Y.S. Bae, H. Oh, S.G. Rhee, Y. Do Yoo, Regulation of reactive oxygen species generation in cell signaling, Mol. Cells 32 (2011) 491–509.
[15] R. De Michele, F. Carimi, W.B. Frommer, Mitochondrial biosensors, Int. J. Biochem. Cell Biol. 48 (2014) 39–44.
[16] J.X. Han, Z. Liu, Y.J. Guo, G.C. Han, W. Li, S.Y. Chen, S.F. Zhang, Determination of superoxide anion radical by modified CdTe quantum dots, J. Photochem. Photobiol., A 349 (2017) 1–6.
[17] N. Warwar, A. Mor, R. Fluhr, R.P. Pandian, P. Kuppusamy, A. Blank, Detection and imaging of superoxide in roots by an electron spin resonance spin-probe method, Biophys. J. 101 (2011) 1529–1538.
[18] R. Michalski, B. Michalowski, A. Sikora, J. Zielonka, B. Kalyanaraman, On the use of fluorescence lifetime imaging and dihydroethidium to detect superoxide in intact animals and ex vivo tissues: a reassessment, Free Radic. Biol. Med. 67 (2014) 278–284.
[19] C.D. Georgiou, I. Papapostolou, K. Grintzalis, Superoxide radical detection in cells, tissues, organisms (animals, plants, insects, microorganisms) and soils, Nat. Protoc. 3 (2008) 1679–1692.
[20] F. Dondurmacioglu, A.N. Avan, R. Apak, Simultaneous detection of superoxide anion radicals and determination of the superoxide scavenging activity of antioxidants using a N,N-dimethyl-p-phenylene diamine/Nafion colorimetric sensor, Anal Methods-Uk 9 (2017) 6202–6212.
[21] Y.L. Liu, X.H. Liu, Y.D. Liu, G.A. Liu, L. Ding, X.Q. Lu, Construction of a highly sensitive non-enzymatic sensor for superoxide anion radical detection from living cells, Biosens. Bioelectron. 90 (2017) 39–45.
[22] M. Fujita, R. Tsuruta, S. Kasaoka, K. Fujimoto, R. Tanaka, Y. Oda, M. Nanba, M. Igarashi, M. Yuasa, T. Yoshikawa, T. Maekawa, In vivo real-time measurement of superoxide anion radical with a novel electrochemical sensor, Free Radic. Biol. Med. 47 (2009) 1039–1048.
[23] X. Zhu, X.H. Niu, H.L. Zhao, J. Tang, M.B. Lan, Immobilization of superoxide dismutase on Pt-Pd/MWCNTs hybrid modified electrode surface for superoxide anion detection, Biosens. Bioelectron. 67 (2015) 79–85.
[24] T.D. Wu, L. Li, G.J. Song, M.M. Ran, X.Q. Lu, X.H. Liu, An ultrasensitive electrochemical sensor based on cotton carbon fiber composites for the determination of superoxide anion release from cells, Microchim Acta 186 (2019).
[25] S.K. Kim, D. Kim, J.M. You, H.S. Han, S. Jeon, Non-enzymatic superoxide anion radical sensor based on Pt nanoparticles covalently bonded to thiolated MWCNTs, Electrochim. Acta 81 (2012) 31–36.
[26] R. Nissim, R.G. Compton, Nonenzymatic electrochemical superoxide sensor, Chemelectrochem 1 (2014) 763–771.
[27] M. Balamurugan, P. Santharaman, T. Madasamy, S. Rajesh, N.K. Sethy, K. Bhargava, S. Kotamraju, C. Karunakaran, Recent trends in electrochemical biosensors of superoxide dismutases, Biosens. Bioelectron. 116 (2018) 89–99.
[28] M. Hayyan, M.A. Hashim, I.M. AlNashef, Superoxide ion: generation and chemical implications, Chem. Rev. 116 (2016) 3029–3085.
[29] A. Prasad, A. Kumar, R. Matsuoka, A. Takahashi, R. Fujii, Y. Sugiura, H. Kikuchi, S. Aoyagi, T. Aikawa, T. Kondo, M. Yuasa, P. Pospisil, S. Kasai, Real-time monitoring of superoxide anion radical generation in response to wounding: electrochemical study, PeerJ 5 (2017), e3050.
[30] M.F.S. Teixeira, M.M. Barsan, C.M.A. Brett, Molecular engineering of a pi-conjugated polymer film of the azo dye Bismarck Brown Y, RSC Adv. 6 (2016) 101318–101322.
[31] L.Y. Chen, Y.H. Tang, K. Wang, C.B. Liu, S.L. Luo, Direct electrodeposition of reduced graphene oxide on glassy carbon electrode and its electrochemical application, Electrochem. Commun. 13 (2011) 133–137.
[32] C.B. Liu, K. Wang, S.L. Luo, Y.H. Tang, L.Y. Chen, Direct electrodeposition of graphene enabling the one-step synthesis of graphene-metal nanocomposite films, Small 7 (2011) 1203–1206.
[33] S. Gupta, C. Price, Investigating graphene/conducting polymer hybrid layered composites as pseudocapacitors: interplay of heterogeneous electron transfer, electric double layers and mechanical stability, Compos. B Eng. 105 (2016) 46–59.
[34] M. Dobbelin, A. Ciesielski, S. Haar, S. Osella, M. Bruna, A. Minoia, L. Grisanti, T. Mosciatti, F. Richard, E.A. Prasetyanto, L. De Cola, V. Palermo, R. Mazzaro, V. Morandi, R. Lazzaroni, A.C. Ferrari, D. Beljonne, P. Samori, Light-enhanced liquid-phase exfoliation and current photoswitching in graphene-azobenzene composites, Nat. Commun. 7 (2016).
[35] V.F. Lvovich, A perspective on electrochemical impedance analysis of polyaniline films on electrodes, Electrochem Soc Inte 18 (2009) 62–66.
[36] Y. Fang, X.B. Tan, G. Alici, Redox level-dependent impedance model for conjugated polymer actuators, Sens. Actuators B Chem. 132 (2008) 182–190.
[37] S.L.G. Lissy, S. Pitchumani, K. Jayakumar, The effect of film thickness and counter ions on the double layer and redox capacitance of polyaniline thin film electrode, Mater. Chem. Phys. 76 (2002) 143–150.
[38] J.F. Rubinson, Y.P. Kayinamura, Charge transport in conducting polymers: insights from impedance spectroscopy, Chem. Soc. Rev. 38 (2009) 3339–3347.
[39] H.X. Ji, X. Zhao, Z.H. Qiao, J. Jung, Y.W. Zhu, Y.L. Lu, L.L. Zhang, A.H. MacDonald, R.S. Ruoff, Capacitance of carbon-based electrical double-layer capacitors, Nat. Commun. 5 (2014).
[40] Y. Gao, Graphene and polymer composites for supercapacitor applications: a review, Nanoscale Res Lett 12 (2017).
[41] S. Skale, V. Dolecek, M. Slemnik, Substitution of the constant phase element by Warburg impedance for protective coatings, Corros. Sci. 49 (2007) 1045–1055.
[42] S. Madhurantakam, S. Selvaraj, N. Nesakumar, S. Sethuraman, J.B.B. Rayappan, U.M. Krishnan, Electrochemical enzymeless detection of superoxide employing naringin-copper decorated electrodes, Biosens. Bioelectron. 59 (2014) 134–139.
[43] M. Braik, M.M. Barsan, C. Dridi, M. Ben Ali, C.M.A. Brett, Highly sensitive amperometric enzyme biosensor for detection of superoxide based on conducting polymer/CNT modified electrodes and superoxide dismutase, Sens. Actuators B Chem. 236 (2016) 574–582.